A Structural Factor Responsible for Substrate Recognition by *Bacillus* sp. GL1 Xanthan Lyase that Acts Specifically on Pyruvated Side Chains of Xanthan[†,‡]

Yukie Maruyama,[§] Bunzo Mikami,[||] Wataru Hashimoto,[§] and Kousaku Murata*[,§]

Laboratory of Basic and Applied Molecular Biotechnology, Division of Food Science and Biotechnology, Graduate School of Agriculture, Kyoto University, Uji, Kyoto 611-0011, Japan, and Laboratory of Applied Structural Biology, Division of Applied Life Science, Graduate School of Agriculture, Kyoto University, Uji, Kyoto 611-0011, Japan

Received September 22, 2006; Revised Manuscript Received November 15, 2006

ABSTRACT: Xanthan is a bacterial heteropolysaccharide composed of pentasaccharide repeating units, i.e., a cellobiose as a backbone and a trisaccharide consisting of two mannoses and one glucuronic acid as a side chain. Nonreducing terminal mannose residues of xanthan side chains are partially pyruvated. *Bacillus* sp. GL1 xanthan lyase, a member of polysaccharide lyase family 8, acts specifically on pyruvated side chains of xanthan and yields pyruvated mannose through a β-elimination reaction by using a single Tyr255 residue as base and acid catalysts. Here we show structural factors for substrate recognition by xanthan lyase through X-ray crystallographic and mutational analyses. The enzyme accommodates mannose and pyruvated mannose at the −1 subsite, although both inhibitor and dissociation constants of the two monosaccharides indicated that the affinity of pyruvated mannose for xanthan lyase is much higher than that of mannose. The high affinity of pyruvated mannose is probably due to the formation of additional hydrogen bonds between the carboxyl group of pyruvated mannose and amino acid residues of Tyr315 and Arg612. Site-directed mutagenesis of the two residues demonstrated that Arg612 is a key residue in recognizing pyruvated mannose. Arg612 is located in the protruding loop covering the substrate, suggesting that the loop functions as a lid that is responsible for the proper accommodation of the substrate at the active site.

Polysaccharide lyases recognize uronic acid residues in polysaccharides, cleave their glycosidic bonds through a β-elimination reaction, and produce unsaturated saccharides with C═C double bonds at nonreducing terminal uronate residues. This suggests the presence of common structural features responsible for catalytic reactions shared in polysaccharide lyases, i.e., uronate recognition and β-elimination reaction. In fact, among polysaccharide lyase families PL-1−18 in the CAZy database (afmb.cnrs-mrs.fr/~cazy/CAZY/index.html), family PL-1 and -10 enzymes have common steric arrangements of catalytic residues despite their distinctive overall structures and amino acid sequences (*1*). The proposed catalytic reaction mechanisms for PL-5, -7, and -8 lyases and a nonclassified lyase, heparinase II, are similar, although no sequence identity is observed (*2*−*7*) among these enymes. Little information about common structural features responsible for substrate recognition has been gathered.

Xanthan is a heteropolysaccharide produced by *Xanthomonas campestris*, a pathogenic plant bacterium (*8*, *9*), and suggested to be involved in causing black rot by this bacterium (*10*, *11*). The polysaccharide consists of pentasaccharide repeating units, i.e., a main cellulosic backbone (cellobiose) with a trisaccharide side chain composed of one glucuronyl (GlcUA)[1] and two mannosyl (Man) residues at C-3 positions of alternate glucosyl residues. Some internal and terminal mannosyl residues of side chains have an *O*-acetyl group at the C-6 position and a pyruvate ketal at the C-4 and C-6 positions (Figure 1). Due to its superior viscosity and stability at low concentrations and over a wide pH range, xanthan is extensively used as a gelling and stabilizing agent in a variety of fields, including the food, oil, and pharmaceutical industries (*12*, *13*). In addition to its excellent rheological properties, it has biological activity such as decreasing serum uric acid and urea nitrogen concentrations and adsorbing cholesterol (*14*, *15*). The production of modified xanthans with altered properties would thus increase the utility of this polymer. In fact, xanthan treated with xanthan lyase has been confirmed in experiments to exhibit excellent food-technology properties (*16*). The molecular and structural biology of xanthan-degrading enzymes such as

[†] This work was supported in part by Grants-in-Aid from the Ministry of Education, Culture, Sports, Science, and Technology of Japan (K.M., B.M., and W.H.) and by Research Fellowships from the Japan Society for the Promotion of Science for Young Scientists (Y.M.). Part of this work was also supported by the Program of Basic Research Activities for Innovative Biosciences (PROBRAIN) of Japan.

[‡] Coordinates of the xanthan lyase−Man complex and R612A have been deposited in the RCSB Protein Data Bank as entries 2E22 and 2E24, respectively.

* To whom correspondence should be addressed. E-mail: kmurata@kais.kyoto-u.ac.jp. Fax: +81-774-38-3767. Phone: +81-774-38-3766.

[§] Division of Food Science and Biotechnology.

[||] Division of Applied Life Science.

[1] Abbreviations: Glc, D-glucose; AcMan, acetylated D-mannose; GlcUA, D-glucuronic acid; PyrMan, pyruvated D-mannose; PDB, Protein Data Bank; rms, root-mean-square; PL, polysaccharide lyase family; KPB, potassium phosphate buffer; Tris, tris(hydroxymethyl)-aminomethane; PEG, polyethylene glycol; Bicine, *N*,*N*-bis(2-hydroxyethyl)glycine; GL1, *Bacillus* sp. GL1; α-domain, N-terminal α-helical domain; β-domain, C-terminal β-sheet domain.

10.1021/bi0619775 CCC: $37.00
Published on Web 12/29/2006

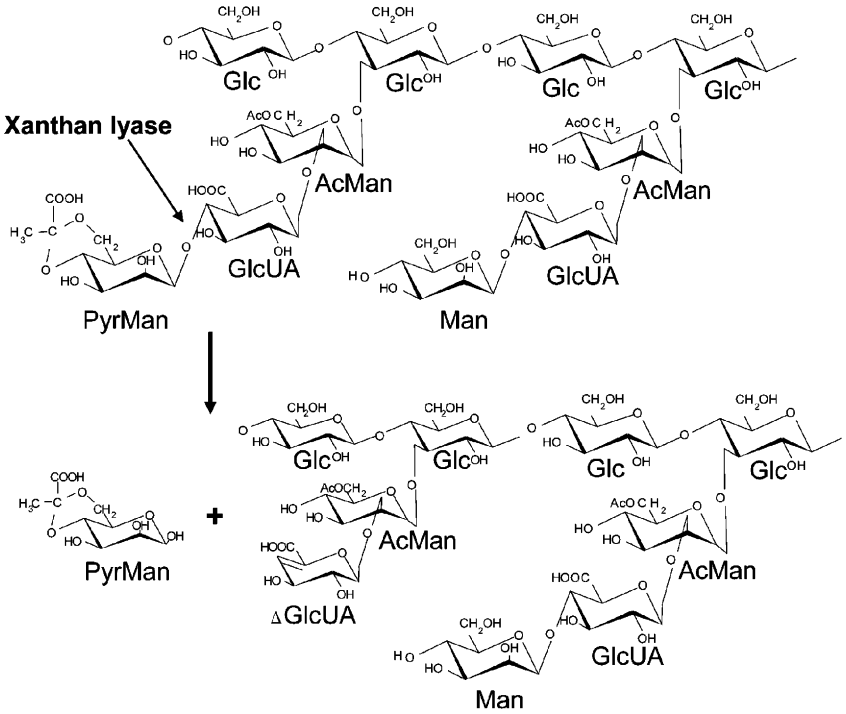

FIGURE 1: Structure of the xanthan polymer and mode of cleavage by xanthan lyase. The thin arrow denotes the cleavage site for xanthan lyase and the thick arrow the degradation reaction. Xanthan lyase liberates PyrMan but not Man.

xanthan lyase is therefore important in the application of modified xanthan to polymer industries and the establishment of a novel therapy for xanthomonas-infectious rot in plants.

Xanthan lyase from *Bacillus* sp. GL1 acts on pyruvated side chains of xanthan and yields pyruvated mannose (PyrMan) and a truncated xanthan polymer through a β-elimination reaction (Figure 1). On the basis of the primary structure, the enzyme is classified into PL-8, including hyaluronate and chondroitin AC lyases. Xanthan lyase does not act on other polysaccharides, such as hyaluronan, chondroitin A, pectin, heparin, gellan, fucoidan, or alginate (*17*). Mannose could not be detected as a product of the enzyme reaction (*17*); i.e., the enzyme specifically recognizes PyrMan. We recently reported on the crystal structure of a mutant xanthan lyase, N194A, complexed with a pentasaccharide substrate (*5*). On the basis of the structural characteristics of the complex, it has been proposed that the enzyme catalyzes the β-elimination reaction by using a single Tyr255 as base and acid catalysts. In addition to the enzyme reaction mechanism, the mode of binding of sugars to the enzyme has been partially realized. At the catalytic site, only two sugars bound at the -1 (PyrMan) and $+1$ (GlcUA) subsites were visible, and the other three sugars were thought to be structurally disordered. The average *B* factors of PyrMan atoms were significantly lower than those of GlcUA, suggesting that PyrMan bound strongly to the enzyme. These facts may indicate that the -1 subsite is crucial for substrate recognition by xanthan lyase. Its substrate recognition mechanism responsible for specificity remains, however, to be clarified.

Both PL-5 and -8 lyases are known to have in common an α/α-barrel fold in their catalytic domain and a reaction mechanism in which a single tyrosine residue acts as base and acid catalysts (*2*, *4*, *5*). In the PL-5 alginate lyase, loop movement is involved in substrate binding and product release (*3*). PL-8 enzymes have no conserved loop structure involved in substrate binding. With hyaluronate lyase, interdomain movements are thought to be important for substrate binding and product release (*18*). The loop movement of chondroitin AC lyase appears to be involved in substrate binding (*4*), although the corresponding loop is absent from other PL-8 enzymes (*5*). Substrate recognition mechanisms of PL-8 enzymes are thus probably specific to each enzyme. To determine how xanthan lyase recognizes the substrate, we determined structures of the ligand-free mutant and the wild-type enzyme in complex with Man bound at the -1 subsite and determined kinetic parameters by using mutant enzymes with a mutation at the active site. This article deals with the clarification of a structural factor responsible for substrate recognition by xanthan lyase. The results we obtained provide valuable information about the structural similarity in substrate recognition between xanthan lyase and PL-5 alginate lyase and the substrate specificity of xanthan lyase.

EXPERIMENTAL PROCEDURES

Materials. Pyruvated xanthan was obtained from Kohjin (Tokyo, Japan). Its molecular mass was 2×10^6 Da, and the degree of pyruvation of the terminal mannosyl residue in side chains was ~50%. PyrMan was purified as described elsewhere (*19*). Man was purchased from Nacalai Tesque (Kyoto, Japan).

Expression and Purification of Wild-Type and Mutant Xanthan Lyases. Escherichia coli cells with the xanthan lyase gene were cultivated and disrupted using the same procedures as described elsewhere (*20*). Briefly, BL21(DE3)pLysS cells with a plasmid (pET17b-XL4) grown in a LB medium at 16 °C were collected by centrifugation at 6000*g* and 4 °C for 5 min, suspended in 20 mM potassium phosphate buffer (KPB, pH 7.0), and then disrupted ultrasonically (Insonator model 201M, Kubota, Tokyo, Japan) at 0 °C and 9 kHz for

20 min. Cell extracts were fractionated with ammonium sulfate. The precipitate of the 0−30% saturation fraction was dissolved in 20 mM KPB (pH 7.0) and then applied to a DEAE-Toyopearl 650M column (Tosoh, Tokyo, Japan) equilibrated with the same buffer. The enzyme was eluted with a linear gradient of NaCl (from 0 to 0.5 M) in 20 mM KPB (pH 7.0). Active fractions, which were eluted at 0.4 M NaCl, were combined and dialyzed against 20 mM KPB (pH 7.0). The dialysate (97 kDa precursor form) was kept at 4 °C for ∼3 months. After confirmation of processing, i.e., conversion of the precursor to the mature form (*20*), the enzyme was applied to a monoQ 10/100 (Amersham Bioscience) column equilibrated with 20 mM KPB (pH 7.0) and eluted with a linear gradient of NaCl (from 0 to 0.5 M) in 20 mM KPB (pH 7.0). Active fractions, which were eluted at 0.4 M NaCl, were combined and dialyzed against 20 mM tris(hydroxymethyl)aminomethane (Tris) HCl (pH 7.5). The dialysate was used as a purified protein.

Protein Measurement. Purified proteins were quantified by measuring the absorbance at 280 nm. The absorption coefficient used for the wild type and all mutant xanthan lyases (E_{280}) was 2.06.

Kinetic Analysis. The activity of xanthan lyase was assayed as described elsewhere (*5*). Briefly, the enzyme was incubated in a 1 mL reaction mixture containing xanthan and 50 mM sodium acetate (pH 5.5) at 30 °C. Different concentrations of xanthan solutions, i.e., 0.05, 0.1, 0.2, 0.4, 0.8, and 1.6 mg/mL, were used for the kinetic study of the wild type, R313A, and Y315F, and 0.25, 0.5, 1, 2, 3, and 4 mg/mL xanthan solutions were used for that of R612A. The enzyme concentration was 0.1 μg/mL. Activity was determined by monitoring the increase in absorbance at 235 nm. K_m and k_{cat} were calculated using the Michaelis−Menten equation with KaleidaGraph (Synergy Software, Reading, PA).

K_i Determination. Inhibition of xanthan lyase activity by PyrMan and Man was assessed. The enzyme assay was conducted with and without sugars (0, 5, and 10 mM PyrMan and 0, 200, and 400 mM Man). Xanthan concentrations used in this assay were 0.1, 0.25, 0.5, 1.0, and 2.0 mg/mL. The enzyme concentration was 0.1 μg/mL in 50 mM sodium acetate (pH 5.5). v^{-1} (v, initial velocity of enzyme activity) was plotted against the sugar concentration in the reaction mixture, and K_i was determined by calculating the intersection of fitting lines.

UV Absorption Difference Spectroscopy. UV absorption difference spectra were obtained with a Shimadzu MPS-2000 spectrophotometer and double-compartment cells; 20 μL of the sugar solution (3.6 M Man or 0.1 M PyrMan) was titrated against the enzyme solution (1 mg/mL). Measurements were taken in 50 mM sodium acetate (pH 5.5).

Fluorescence Studies. The fluorescence was measured on a JASCO spectrofluorophotometer (model FP-6500). Emission spectra of the fluorescence of tryptophans upon excitation at 280 nm were detected between 300 and 400 nm. The enzyme concentration was 0.04 mg/mL; 20 μL of the sugar solution (3.6 M Man or 0.1 M PyrMan) was titrated. Measurements were taken in 50 mM sodium acetate (pH 5.5).

Crystallization and Data Collection. Crystals were prepared by hanging-drop vapor diffusion. Single crystals of wild-type and R612A enzymes were grown at 20 °C in a mixture of enzyme, 22% polyethylene glycol 4000 (PEG4000) (Nacalai Tesque), 0.2 M ammonium formate, and 0.1 M *N*,*N*-bis(2-hydroxyethyl)glycine (Bicine) (pH 9.0). The initial protein concentration was 7 mg/mL. To structurally determine the wild-type enzyme−Man complex, crystals were soaked at 20 °C for 60 min in 100 mM Man in solution A [0.1 M Tris-HCl (pH 7.4), 24% PEG4000, and 0.2 M ammonium formate]. Diffraction data for the Man-soaked xanthan lyase crystal were collected with a Bruker Hi-Star multiwire area detector at 20 °C using Cu Kα radiation generated with a MAC Science M18XHF rotating anode generator and then processed with SADIE and SAINT software (Bruker, Karlsruhe, Germany). A crystal of R612A was flash-cooled under a cold nitrogen stream using 20% PEG400 in solution A as a cryoprotectant. Diffraction data for the R612A crystal were collected at $\lambda = 1$ Å using a Jupiter 210 CCD detector at the BL38B1 Station of SPring-8 (Hyogo, Japan) and processed with HKL2000 (*21*)

Structure Refinement and Manipulation. Coordinates of ligand-free xanthan lyase obtained from the Protein Data Bank (PDB; entry 1J0M) were used as the initial model of wild-type xanthan lyase complexed with Man and the R612A mutant. A randomly selected 5% of the reflections were excluded from refinement and used to calculate R_{free}. After each cycle of energy minimization and *B* factor refinement with CNS (*22*), models were adjusted manually using Turbo-Frodo (AFMB-CNRS). Isolated electron densities exceeding 3σ on the $F_o - F_c$ map and/or 1.2σ on the $2F_o - F_c$ map were assigned as water molecules when their locations were sterically reasonable. PyrMan complex data were collected and described previously (*19*) and re-refined here using another restraint parameter for PyrMan. Diffraction data and coordinates of xanthan lyase complexed with PyrMan were obtained from PDB (entry 1J0N). The structure was re-refined using CNS with the parameter file for PyrMan at the PRODRG site (http://davapc1.bioch.dundee.ac.uk). Cis peptide restrictions were added to peptide bonds between Tyr145 and Asn146, Ala338 and Pro339, and Ala753 and Pro754 (*5*, *19*). The final model quality was checked with PROCHECK (*23*). We superimposed protein models and calculated their root-mean square (rms) deviation with LSQKAB (*24*), part of the CCP4 suite (*25*, *26*). Hydrogen bonds and C−C contacts between the enzyme and sugar atoms were evaluated using CONTACT in CCP4 (*25*). Figures for protein structures were prepared using Molscript (*27*) with Raster3D (*28*), Bobscript (*29*) with Raster3D (*25*), Turbo-Frodo (AFMB-CNRS), or MolFeat (FiatLux, Tokyo, Japan).

Site-Directed Mutagenesis. To substitute Arg313, Tyr315, and Arg612 for Ala, Phe, and Ala, respectively, we synthesized the following six oligonucleotides: R313A sense primer, 5′-GCGCGGACGGGAGATTTCCGCCAGCTACG-CGCAGG-3′; R313A antisense primer, 5′-CCTGCGCG-TAGCTGGCGGAAATCTCCCGTCCGCGC-3′; Y315F sense primer, 5′-GGAGATTTCCCGCAGCTTCGCGCAGGAT-CATGCGG-3′; Y315F antisense primer, 5′-CCGCATGATC-CTGCGCGAAGCTGCGGGAAATCTCC-3′; R612A sense primer, 5′-GGAAGCAGATCAACAATGCCCCGGCCACG-CCCTCTACC-3′; and R612A antisense primer, 5′-GGTA-GAGGGCGTGGCCGGGGCATTGTTGAT-CTGCTTCC-3′. Underlining in oligonucleotide sequences indicates the position of mutations. Site-directed mutagenesis was conducted using plasmid pET17b-XL4 (*20*) as a template and synthetic oligonucleotides as sense and antisense primers

Table 1: Inhibitor Constants of Xanthan Lyases

	K_i (mM)	
	PyrMan	Man
wild type	2.21 ± 1.22	837 ± 113
R612A	19.2 ± 1.35	410 ± 39.3

according to the manufacturer's directions (Stratagene Co.) for a Quick Change site-directed mutagenesis kit. Resulting plasmids with mutations were designated as pR313A, pY315F, and pR612A. Mutations were confirmed by DNA sequencing. Cells of the *E. coli* host strain [BL21(DE3)-pLysS] were transformed with plasmids pR313A, pY315F, and pR612A.

DNA Sequence and DNA Manipulation. Nucleotide sequences of xanthan lyase genes were determined by dideoxy chain termination using a model 377 automated DNA sequencer (Applied Biosystems Division, Perkin-Elmer) (*30*). Subcloning, transformation, and gel electrophoresis were conducted as described elsewhere (*31*).

RESULTS

Sugar Binding Affinity of Xanthan Lyase. To clarify the difference in affinity for xanthan lyase between Man and PyrMan, we assessed inhibition of the enzyme reaction by these sugars. Enzyme activity was inhibited proportionally with respect to the concentration of sugar added, indicating that Man also binds to xanthan lyase. The mechanism of the inhibition seems to be competitive rather than uncompetitive or noncompetitive. On the basis of the Dixon plot, we estimated inhibitor constants (Table 1). The affinity of PyrMan was ~400 times stronger than that of Man. Dissociation constants (K_d) of PyrMan and Man for dissociation from xanthan lyase were also estimated from the fluorescence of tryptophan residues with excitation at 280 nm and by UV absorption difference spectroscopy at 280 nm. Fluorescence decreased with the increased concentration of sugar titrated, yielding a saturation curve. Dissociation constants were estimated to be 10.1 ± 0.40 mM for PyrMan and 419 ± 89 mM for Man. Similarly, absorbance at 280 nm decreased with titration of the sugar solution. The K_d estimated from the titration curve was 8.98 ± 0.35 mM for PyrMan and 444 ± 71 mM for Man, agreeing well with fluorescence experiment results. These results indicate that the affinity of PyrMan for xanthan lyase is much stronger than that of Man.

Crystal Structures of Xanthan Lyases Complexed with PyrMan and Man. Xanthan lyase consists of two distinct structural domains connected by a short polypeptide linker, i.e., an N-terminal α-helical domain (α-domain) and a C-terminal *β*-sheet domain (*β*-domain). The α-domain contains 13 helices arranged in an $(\alpha/\alpha)_5$-barrel structure. The *β*-domain is predominantly composed of five antiparallel *β*-sheets. The protein structure is detailed elsewhere (*19*).

To determine how xanthan lyase distinguishes structures of PyrMan and Man at the −1 subsite, we determined the crystal structure of xanthan lyase complexed with Man at 2.4 Å resolution (Figure 2a). The structure of the enzyme−Man complex was refined to a model with good geometry and crystallographic quality. Table 2 summarizes the data collection of and refinement statistics for xanthan lyase complexed with Man. The overall structure of the enzyme−Man complex is comparable to structures, reported elsewhere, of ligand-free and PyrMan-bound xanthan lyases (*19*). The density peak for Man was observed at the −1 subsite of the catalytic cleft located at one end of the α-domain (Figure 2a,b) as seen in the enzyme−PyrMan complex (Figure 2c).

Prior to structural comparison with the enzyme−PyrMan complex, we re-refined its structure because the sugar ring conformation of PyrMan in the previous wild type−PyrMan complex was somewhat distorted. Higher-resolution analysis of the N194A−PyrMan complex showed that this ring formed a stable chair conformation. These differences are thought to be due to the parameter files used for structure refinement (*5*). After re-refinement, the sugar ring of PyrMan was found to form a chair conformation in the wild type−PyrMan complex as seen in the N194A−PyrMan complex, while little conformational difference was observed in the pyruvated group of the sugar and amino acid residues of the enzyme.

Comparison of Active Site Structures. Figure 2d shows superimposed structures of xanthan lyases complexed with PyrMan and Man. The rms deviation for all C^α atoms is 0.14 Å, suggesting that the enzyme binds to Man without conformational change. The locations of Man and PyrMan are essentially the same. The conformation and direction of the Man pyranose ring are very similar to those of PyrMan.

To find out what determines the difference in affinity of the enzyme for PyrMan and Man, we compared active site structures of complexes for PyrMan and Man (Figure 3). Close contacts between sugar and protein or water atoms are listed in Table 3. The sugar pyranose ring is stacked with Trp148. Tyr255 and Arg309 form hydrogen bonds with O-1 atoms of PyrMan and Man, which accept a proton from a general base catalyst through the enzyme reaction. The guanidinium group of Arg309 also contacts the O-2 atom. Arg313 interacts with O-2 and O-3 atoms. These contacts are all the same in xanthan lyase in complexes with PyrMan and Man, indicating similar modes of binding to xanthan lyase. Differences arise in interactions between the pyruvate group and amino acid residues. Both the hydroxyl group of Tyr315 and the guanidinium group of Arg612 form hydrogen bonds with the carboxyl group of PyrMan. These hydrogen bonds are not formed in the enzyme−Man complex because of the lack of a pyruvate group. In contrast, interaction between the O-6 atom of Man and $N^{\eta 1}$ of Arg612 occurs particularly in the enzyme−Man complex.

Mutation Analyses. As indicated in Table 3, Tyr315 and Arg612 are residues that form hydrogen bonds with the pyruvate group of sugar in the enzyme−PyrMan complex but not in the enzyme−Man complex. Conformational differences between structures before and after rerefinement indicate that there are some biases in the restraint parameters that are used. We therefore carefully investigated other residues probably interacting with the pyruvated group of PyrMan. Arg313 is also a possible residue interacting with the PyrMan carboxyl group; the distance between $N^{\eta 1}$ of Arg313 and O-7 of PyrMan is 3.5 Å. We substituted Arg313, Tyr315, and Arg612 for Ala, Phe, and Ala, respectively, and studied the effect of mutation on enzymatic activity. Kinetic parameters of mutants R313A, Y315F, and R612A are summarized in Table 4. R313A decreased k_{cat} dramatically but did not change K_m, suggesting that this residue is important for catalysis, which appears to be reasonable

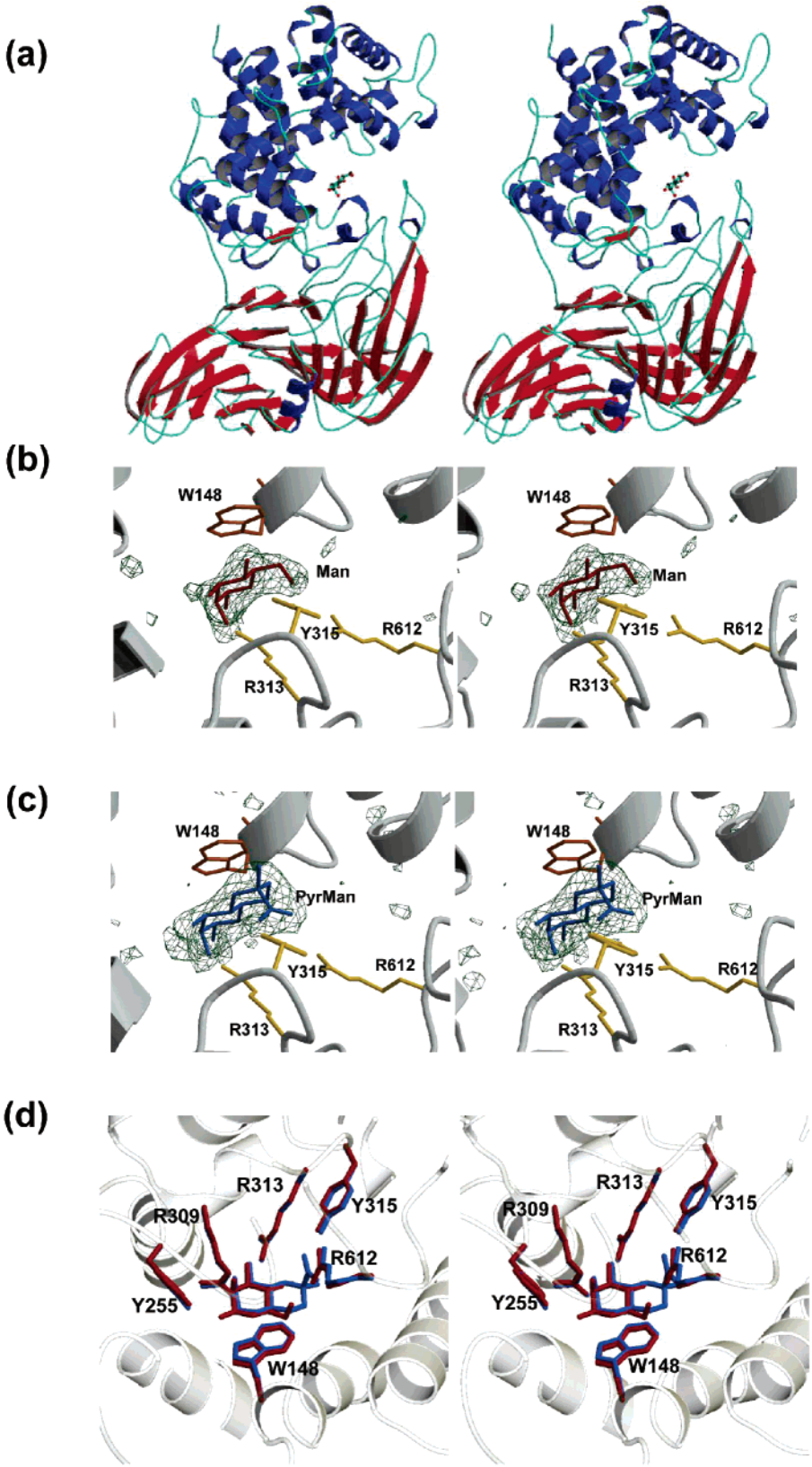

FIGURE 2: Stereo crystal structures of xanthan lyases complexed with monosaccharides: (a) overall structure of xanthan lyase complexed with Man, electron density map at the active site of xanthan lyase complexed with Man (b) and PyrMan (c), and the superimposition of two xanthan lyases complexed with monosaccharides (d). Electron density maps colored green ($F_o - F_c$, contoured at 3σ) were calculated using models without sugars. Blue and red in panel d represent structures of the enzyme complexed with PyrMan and Man.

because the loss of interaction of the Arg313 side chain with O-2 and O-3 atoms of the PyrMan pyranose ring may cause an unstable conformation at the catalytic site. Conservation of the Arg313 sequence and conformation in polysaccharide lyase family 8 (PL-8) enzymes, including lyases for xanthan, hyaluronan, and chondroitin AC (*19*), also supports the importance of this residue in catalysis. Compared to that of the wild-type enzyme, the k_{cat} of Y315F did not change

Table 2: Data Collection and Refinement Statistics for Wild-Type and Mutant Xanthan Lyases

	wild type−Man	wild type−PyrMan[b]	R612A
crystal data			
X-ray source	Cu Kα	Cu Kα	SPring-8 BL38B1
space group	$P2_12_12_1$	$P2_12_12_1$	$P2_1$
cell dimensions	$a = 54.36$ Å, $b = 91.46$ Å, $c = 159.65$ Å	$a = 54.36$ Å, $b = 91.31$ Å, $c = 159.26$ Å	$a = 53.81$ Å, $b = 90.23$ Å, $c = 78.10$ Å, $\beta = 97.56°$
no. of molecules per asymmetric unit	1	1	1
resolution range (Å)	∞−2.36 (2.45−2.36)[a]	26.3−2.40 (2.49−2.40)[a]	50−2.15 (2.23−2.15)[a]
no. of observed reflections	99615	55703	221980
no. of unique reflections	29738	28677	39353
completeness (%)	88.6 (42.9)[a]	89.9 (73.7)[a]	97.3 (77.8)[a]
R_{merge}	0.064 (0.254)[a]	0.091 (0.376)[a]	0.113 (0.324)[a]
refinement data			
resolution range (Å)	50−2.4 (2.49−2.40)[a]	50−2.4 (2.49−2.40)[a]	50−2.15 (2.23−2.15)[a]
average B factor (Å^2)			
amino acid residues	24.5	21.9	18.7
water molecules	27.8	21.4	25.3
calcium ions	−	26.7	−
saccharides	29.9	19.6	−
PEGs	−	−	28.0
R factor			
R_{cyst}	0.165 (0.230)[a]	0.170 (0.288)[a]	0.174 (0.2073)[a]
R_{free}	0.210 (0.299)[a]	0.215 (0.326)[a]	0.218 (0.2384)[a]
no. of atoms			
amino acid residues	5697	5697	5689
water molecules	230	217	559
calcium ions	0	1	0
saccharides	12	17	0
PEG	0	0	7
rms deviation from ideality			
bond lengths (Å)	0.005	0.006	0.005
bond angles (deg)	1.25	1.29	1.25
Ramachandran plot			
most favored (%)	88.2	87.8	86.7
disallowed (%)	0.2	0.2	0.2

[a] Data for highest-resolution shells are given in parentheses. [b] Data statistics are cited from a previous report (*19*).

significantly and the K_m was increased slightly. The K_m of R612A increased dramatically. The high K_m of R612A made the kinetic assay difficult because the reaction solution became viscous and absorbance at 235 nm increased with xanthan concentration. Substrate concentrations used for kinetically assaying R612A ranged from 0.25 to 4.0 mg/mL, which are insufficient for determining exact K_m and k_{cat} values for R612A, which accounts for the large error in parameters for R612A. It is certain, in any case, that the K_m of R612A is much higher than that of the wild-type enzyme. The increase in K_m indicates a decrease in affinity between the substrate and R612A. Using inhibition analysis, we studied the sugar affinity of R612A. The inhibitor constant of PyrMan for R612A was estimated to be 19.2 mM (Table 1), which is 9 times higher than that for the wild-type enzyme, suggesting a low affinity between PyrMan and R612A. The affinity of R612A with Man increased compared to that of the wild type with Man (Table 1).

Crystal Structure of R612A. To investigate the effect of mutation on higher-order structures, the crystal structure of R612A was determined (Table 2). The overall structure of R612A is equivalent to that of wild-type xanthan lyase. Despite the good quality of crystallographic data and refinement statistics, electron density maps for A612 and its neighbor were poor (Figure 4a). In contrast, corresponding maps for the wild type (Figure 4b) and N194A (Figure 4c) were clear. The space group and diffraction data collection of R612A differed from those of the wild-type enzyme but were the same as those of N194A (*5*), indicating that the flexibility of this region in R612A was due to the mutation of Arg612 to Ala.

DISCUSSION

We have structurally clarified modes of binding of xanthan lyase to PyrMan and Man, finding binding positions and conformations of PyrMan and Man to be very similar. No significant difference was observed in surrounding amino acid conformations. Differences were mainly due to the presence or absence of a pyruvate group. Specifically, the hydrogen bond formed between the carboxyl group of PyrMan and Tyr315 or Arg612 in the enzyme−PyrMan complex was not observed in the enzyme−Man complex. R612A significantly increased K_m for the xanthan polymer and K_i for PyrMan, suggesting that the side chain of the arginine residue is responsible for the affinity between xanthan lyase and PyrMan.

Xanthan lyase is classified into PL-8 in the CAZy database. The overall structure of xanthan lyase consisting of α- and β-domains and its active site architecture are common in lyases belonging to this family, such as lyases for hyaluronate (*32*, *33*) and chondroitin AC (*4*, *34*, *35*). Hyaluronate lyase without the β-domain has been reported to still be active (12% of wild-type enzyme activity) (*36*), indicating that the α-domain alone is sufficient for enzyme activity. The role of the β-domain of family PL-8 enzymes remains unknown. As in the case of R612A in this study, a mutant of hyaluronate lyase, N580G, dramatically increased K_m (*37*). Asn580 is the only residue in the β-domain of

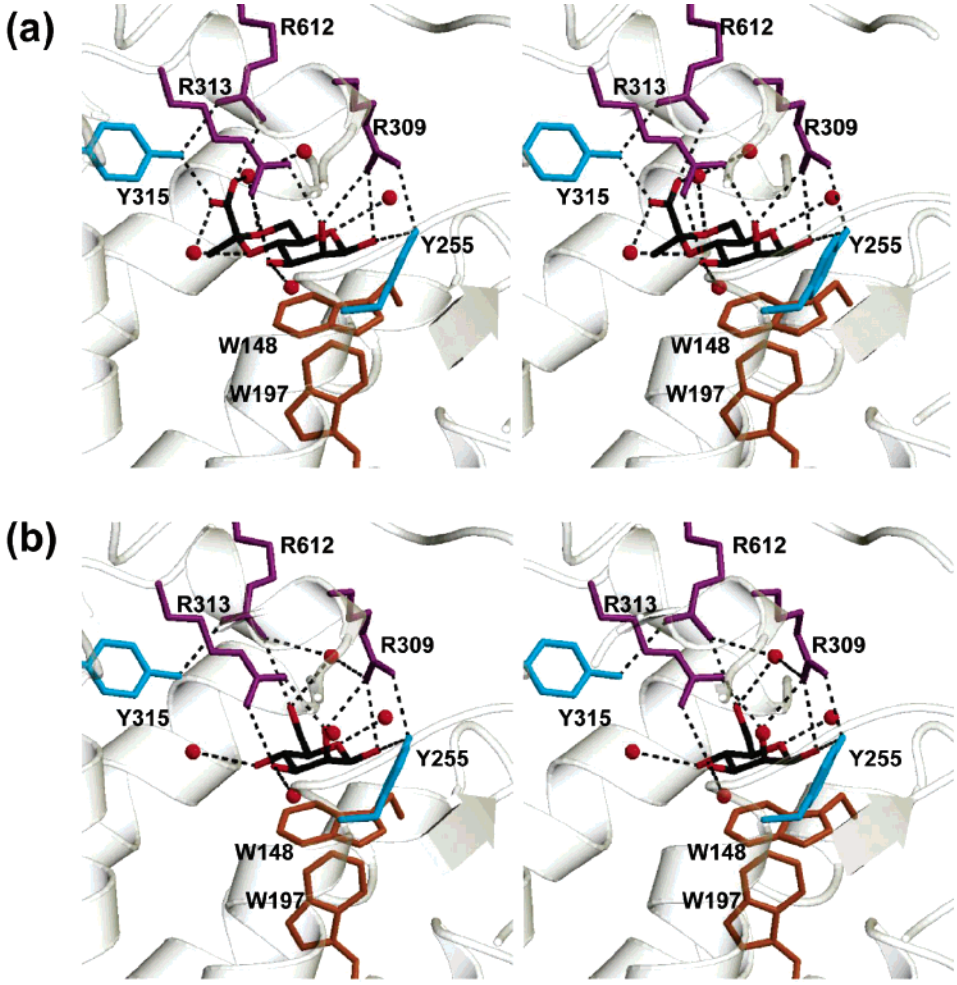

FIGURE 3: Interaction between xanthan lyase and monosaccharides. Stereodiagrams of the active site structure of xanthan lyase complexed with PyrMan (a) and Man (b). Sugar carbon atoms are colored gray and oxygen atoms red. Hydrogen bonds between amino acid residues and sugar residues are represented by dashed lines.

Table 3: Close Contacts between Xanthan Lyase or Water Molecules and Bound Sugar Atoms

sugar atom	protein or water atom	distance[a] (Å) wild type−PyrMan complex	distance[a] (Å) wild type−Man complex
O-1	Tyr255 O^{η}	2.9	2.7
O-1	Arg309 $N^{\eta 2}$	3.2	3.3
O-2	Arg309 $N^{\eta 2}$	3.2	2.9
O-2	Arg313 $N^{\eta 2}$	3.0	2.9
O-2	water		2.6 (230)[b]
O-3	Arg313 $N^{\eta 1}$	3.2	3.1
O-3	water	2.7 (43)[b]	2.8 (43)[b]
O-4	water	2.9 (161)[b]	3.2 (178)[b]
O-5	water	3.2 (123)[b]	2.9 (127)[b]
O-6	Trp148 $C^{\zeta 3}$	3.3	
O-6	water	3.2 (155)[b]	
O-6	water		3.0 (112)[b]
O-6	Arg612 $N^{\eta 1}$		3.3
C-6	water	3.3 (203)[b]	
O-7	Tyr315 O^{η}	2.5	
O-7	water	2.7 (161)[b]	
O-8	Arg612 $N^{\eta 1}$	3.0	
O-8	water	2.7 (155)[b]	

[a] Distance of ≤3.3 Å. [b] Numbers of water molecules are given in parentheses.

Table 4: Kinetic Parameters of Xanthan Lyases

	K_m (mg/mL)	k_{cat} (s^{-1})	k_{cat}/K_m mg^{-1} mL s^{-1}	k_{cat}/K_m %
wild type	0.25 ± 0.015	2170 ± 44	8680	100
R313A	0.37 ± 0.071	9.92 ± 0.67	26.8	0.31
Y315F	0.46 ± 0.068	1730 ± 84	3760	43
R612A	2.9 ± 0.44	6120 ± 500	2110	24

hyaluronate lyase that directly contacts the substrate and is thought to regulate access of the substrate to the enzyme (*37*). Asn424 of xanthan lyase corresponding to Asn580 of hyaluronate lyase is a residue in the loop, termed LB3, that lies along the active site cleft of the enzyme and interacts with the GlcUA residue of the substrate (*5*). In addition to LB3, another loop, LB16, from the β-domain participates in active site formation in xanthan lyase (*19*). Arg612 is a residue in loop LB16. Compared to other PL-8 enzymes, LB16 is specific to xanthan lyase (*5*, *19*). Because Arg612 forms the edge of the −1 subsite, the border of the −1 subsite is open more widely in R612A than in the wild-type enzyme. Distinct from the case of the N580G mutant of hyaluronate lyase, this substitution has no influence on the accessibility of the xanthan polymer in xanthan lyase, since the main chain of xanthan appears to lie along the surface of the "+" subsite of the enzyme (*5*) and xanthan is too large to enter the subsite from the "−" side. Table 1 shows that the substitution of Arg612 with Ala strengthens the affinity of the enzyme for

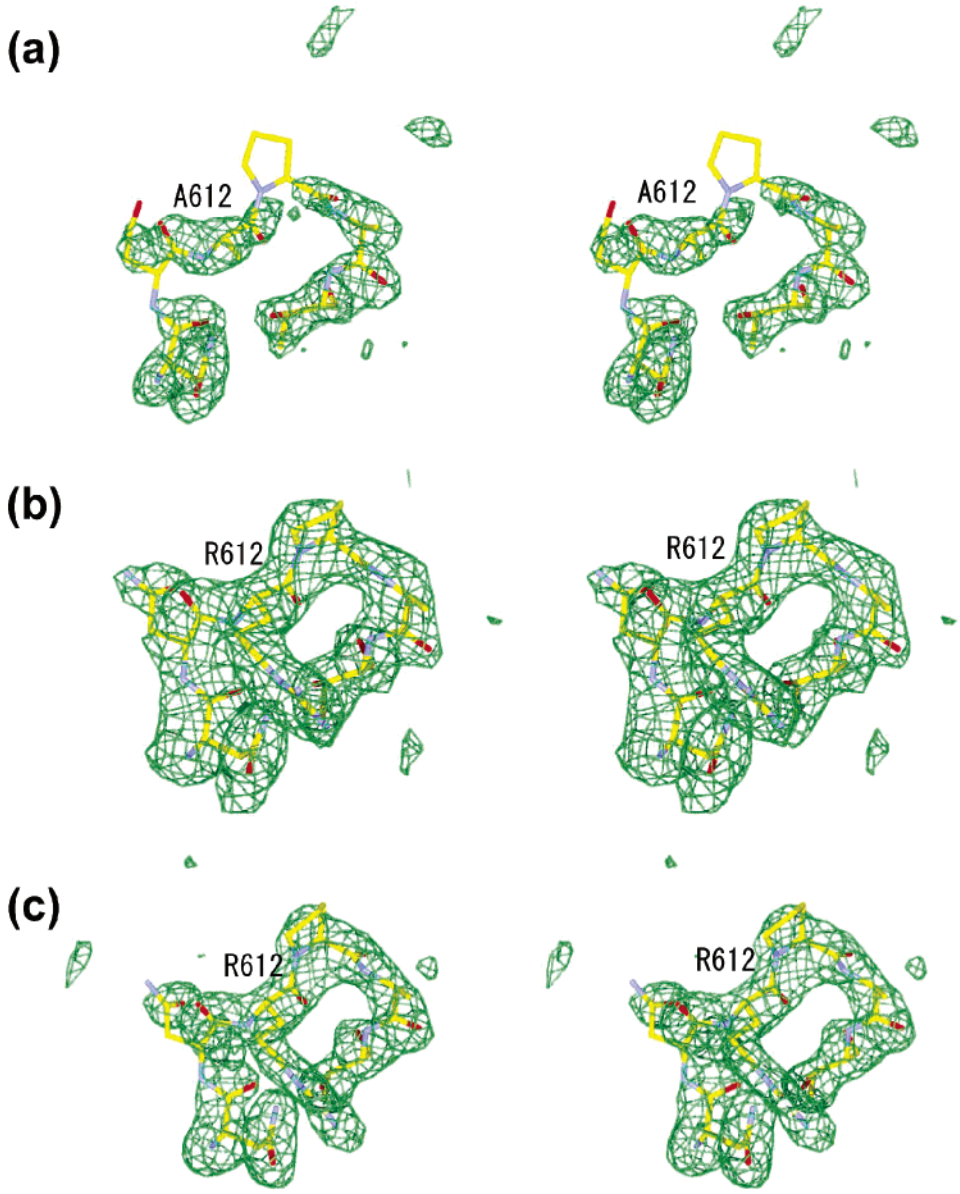

FIGURE 4: Stereoview of the electron density maps ($F_o - F_c$, contoured at 3σ) for Arg612 and its neighbor in R612A (a), wild type (b), and N194A (c). Electron density maps were calculated using models without residues 610−615. This figure was drawn using MolFeat (FiatLux).

Man. Increased affinity with Man in R612A is probably due to the easier access of Man because it lacks the long side chain of Arg612 at the −1 subsite.

It is known that the overall structure and active site conformation of PL-5 alginate lyase (A1-III) from *Sphingomonas* sp. A1 greatly resemble those of α-domains of PL-8 enzymes (*19*, *38*, *39*). In SCOP (http://scop.mrc-lmb.cam.ac.uk/scop/), a database for the structural classification of proteins, the complete structure of PL-5 alginate lyase and the α-domain structure of PL-8 lyases are classified into the same family. When the A1-III structure is superimposed onto that of the α-domain of xanthan lyase using the DALI server (http://www.ebi.ac.uk/dali/), their entire tertiary structures overlapped well. Coordinates were further fitted using C^α atoms within 2.0 Å by RIGID included in Turbo-Frodo (AFMB-CNRS) (Figure 5a). Their rms deviation was 1.4 Å (for 127 C^α atoms). The lid loop covers the active site cleft in the A1-III−product complex and moves away when product is released. This loop movement is involved in substrate binding and catalysis (*3*). The corresponding loop is absent from the α-domain of xanthan lyase. Compared to the lid loop of A1-III, however, LB16 in xanthan lyase protrudes from the opposite side and occupies a similar position (Figure 5a). In addition to the overall structure of the catalytic α-domain and the lid loop structure, several structural features are common to lyases for xanthan and alginate. Intrinsic catalysts, tyrosine residues, and products binding at the −1 subsite in the two lyases superimpose well (Figure 5a,b). As shown in Figure 5b, additional important residues, histidines and asparagines (*2*, *5*), which interact with uronate residues at +1 subsites, are common between the two, although the positions of these residues differ. The Trp148 side chain in xanthan lyase that stacks with the pyranose ring of PyrMan at the −1 subsite corresponds to the Trp141 side chain in A1-III (Figure 5b). These structural similarities suggest that LB16 in xanthan lyase functions as a lid loop responsible for fixation of the structure.

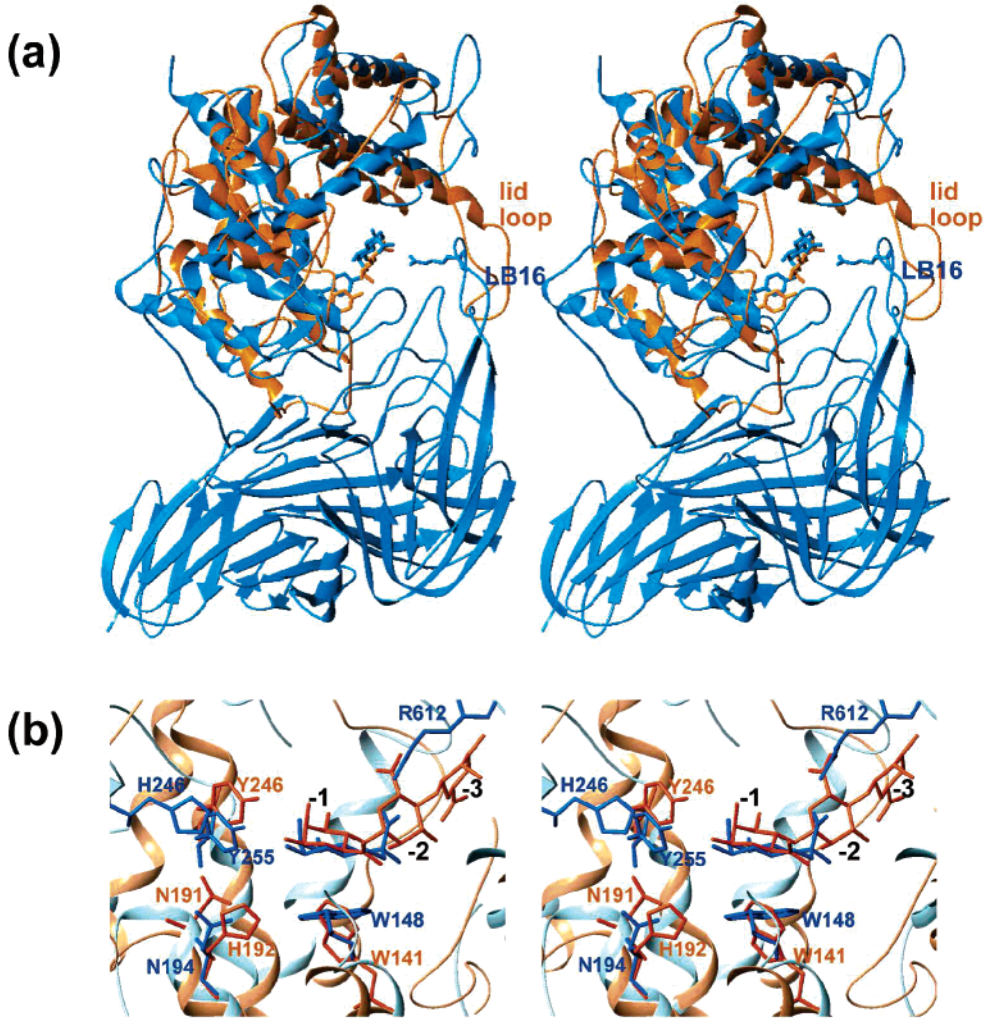

FIGURE 5: Structural comparison between PL-5 and -8 lyases. Stereoscopic comparison of overall (a) and active site (b) structures between PL-5 alginate lyase (A1-III, orange) and xanthan lyase (blue). Coordinates for A1-III were obtained from PDB (entry 1HV6). Proposed catalytic residues (Tyr246 in A1-III and Tyr255 in xanthan lyase) and bound sugars at the −1 subsite (β-D-mannuronate for A1-III and PyrMan for xanthan lyase) overlap well. Loop LB16 of the β-domain of xanthan lyase occupies a position similar to that of the flexible lid loop of A1-III. Catalytically important amino acid residues, Trp, His, and Asn, are also in both despite the nonconserved position. This figure was prepared using Turbo-Frodo.

There are two main reasons that replacement of Arg612 with Ala decreases substrate affinity. First, loop LB16 containing Arg612 is involved in substrate binding as described above (Figure 5a). Interactions of the Arg612 side chain with other amino acid residues, including a hydrogen bond between Arg612 and Tyr315 (Figure 3), may be necessary to maintain the rigid conformation of loop LB16 on the enzyme surface. The lack of these interactions in R612A results in the flexible conformation of LB16 (Figure 4a). Second, arginine residues lining the active site of enzymes are often crucial for binding acidic substrates and determine substrate specificity at subsites (*40*−*42*). Due to the lack of the positive charge of the arginine residue in R612A, the mutant fails to bind to the PyrMan carboxyl group. Either or both of the two are probably responsible for the decrease in substrate affinity when Arg612 is replaced with Ala.

Structural similarity between xanthan lyases complexed with PyrMan and Man also suggests the possibility that the glycoside bond between Man and GlcUA in xanthan can be cleaved when the substrate concentration is sufficiently high in the reaction mixture. Considering the low affinity between Man and xanthan lyase and the inhibition by PyrMan, we investigated whether xanthan lyase yields Man from high-concentration, chemically depyruvated pentasaccharide of xanthan. Mannose was not, however, detected as a product (data not shown). These results suggest that in addition to the differences in affinity between PyrMan and Man for xanthan lyase determined mainly by Arg612, other factors involved in substrate specificity may be present. The substrate structure itself is probably important for xanthan lyase activity. One significant difference between Man and PyrMan structures is that CH_2OH in Man is fixed by the pyruvate ketal in PyrMan. CH_2OH in Man is flexible so that its hydroxyl group can interact with the carboxyl group of GlcUA. The higher-order structure of xanthan is also thought to be altered depending on the side chain modification, as suggested by a molecular simulation study of xanthan with and without acetylation (*43*). All xanthan lyases that have been purified from different microbes and characterized thus far are PyrMan-specific (*17*, *44*, *45*), supporting the importance of a higher-order structure of xanthan for lyase activity.

ACKNOWLEDGMENT

We thank Mr. Sukmyung Yi and Ms. Misato Momma for their assistance in experiments.

REFERENCES

1. Charnock, S. J., Brown, I. E., Turkenburg, J. P., Black, G. W., and Davies, G. J. (2002) Convergent evolution sheds light on the anti-β-elimination mechanism common to family 1 and 10 polysaccharide lyases, *Proc. Natl. Acad. Sci. U.S.A. 99*, 12067−12072.
2. Yoon, H.-J., Hashimoto, W., Miyake, O., Murata, K., and Mikami, B. (2001) Crystal structure of alginate lyase A1-III complexed with a trisaccharide product at 2.0 Å resolution, *J. Mol. Biol. 307*, 9−16.
3. Mikami, B., Suzuki, S., Yoon, H.-J., Miyake, O., Hashimoto, W., and Murata, K. (2002) X-ray structural analysis of alginate lyase A1-III mutants/substrate complexes: Activation of a catalytic tyrosine residue by a flexible lid loop, *Acta Crystallogr. A58*, C271.
4. Lunin, V. V., Li, Y., Linhardt, R. J., Miyazono, H., Kyogashima, M., Kaneko, T., Bell, A. W., and Cygler, M. (2004) High-resolution crystal structure of *Arthrobacter aurescens* chondroitin AC lyase: An enzyme-substrate complex defines the catalytic mechanism, *J. Mol. Biol. 337*, 367−386.
5. Maruyama, Y., Hashimoto, W., Mikami, B., and Murata, K. (2005) Crystal structure of *Bacillus* sp. GL1 xanthan lyase complexed with a substrate: Insights into the enzyme reaction mechanism, *J. Mol. Biol. 350*, 974−986.
6. Yamasaki, M., Ogura, K., Hashimoto, W., Mikami, B., and Murata, K. (2005) A structural basis for depolymerization of alginate by polysaccharide lyase family-7, *J. Mol. Biol. 352*, 11−21.
7. Shaya, D., Tocilj, A., Li, Y., Myette, J., Vankataraman, G., Sasisekharan, R., and Cygler, M. (2006) Crystal structure of heparinase II from *Pedobacter heparinus* and its complex with a disaccharide product, *J. Biol. Chem. 281*, 15525−15535.
8. Rogovin, S. P., Anderson, R. F., and Cadmus, M. C. (1961) Production of polysaccharide with *Xanthomonas campestris*, *J. Biochem. Microbiol. Technol. Eng. 3*, 51−63.
9. Jansson, P.-E., Kenne, L., and Lindberg, B. (1975) Structure of the extracellular polysaccharide from *Xanthomonas campestris*, *Carbohydr. Res. 45*, 275−282.
10. Barber, C. E., Tang, J. L., Feng, J. X., Pan, M. Q., Wilson, T. J., Slaer, H., Dow, J. M., Williams, P., and Daniels, M. J. (1997) A novel regulatory system required for pathogenicity of *Xanhomonas campestris* is mediated by a small diffusible signal molecule, *Mol. Microbiol. 24*, 555−566.
11. Chou, F.-I., Chou, H.-C., Lin, Y.-S., Yang, B.-Y., Lin, N.-T., Weng, S.-F., and Tseng, Y.-H. (1997) The *Xanthomonas campestris* gumD gene required for synthesis of xanthan gum is involved in normal pigmentation and virulence in causing black rot, *Biochem. Biophys. Res. Commum. 233*, 265−269.
12. Morris, V. J. (1995) Bacterial polysaccharides, in *Food polysaccharides and their applications* (Stephan, A. M., Ed.) pp 341−375, Marcel Dekker, New York.
13. Becker, A., Katzen, F., Puhler, A., and Ielpi, L. (1998) Xanthan gum biosynthesis and application: A biochemical/genetic perspective, *Appl. Microbiol. Biotechnol. 50*, 145−152.
14. Soh, H.-S., Kim, C.-S., and Lee, S.-P. (2003) A new in vitro assay of cholesterol adsorption by food and microbial polysaccharides, *J. Med. Food 6*, 225−230.
15. Koguchi, T., Koguchi, H., Nakajima, H., Takano, S., Yamamoto, Y., Innami, S., Maekawa, A., and Tadokoro, T. (2004) Dietary fiber suppresses elevation of uric acid and urea nitrogen concentrate ions in serum of rats with renal dysfunction induced by dietary adenine, *Int. J. Vitam. Nutr. Res. 74*, 253−263.
16. Miki, H. (1999) Master's Thesis. Kyoto University, Kyoto, Japan.
17. Hashimoto, W., Miki, H., Tsuchiya, N., Nankai, H., and Murata, K. (1998) Xanthan lyase of *Bacillus* sp. strain GL1 liberates pyruvated mannose from xanthan side chains, *Appl. Environ. Microbiol. 64*, 3765−3768.
18. Rigden, D. J., Littlejohn, J. E., Joshi, H. V., de Groot, B. L., and Jedrzejas, M. J. (2006) Alternate structural conformations of *Streptococcus pneumoniae* hyaluronan lyase: Insights into enzyme flexibility and underlying molecular mechanism of action, *J. Mol. Biol. 358*, 1165−1178.
19. Hashimoto, W., Nankai, H., Mikami, B., and Murata, K. (2003) Crystal structure of *Bacillus* sp. GL1 xanthan lyase, which acts on the side chains of xanthan, *J. Biol. Chem. 278*, 7663−7673.
20. Hashimoto, W., Miki, H., Tsuchiya, N., Nankai, H., and Murata, K. (2001) Polysaccharide lyase: Molecular cloning, sequencing, and overexpression of the xanthan lyase gene of *Bacillus* sp. strain GL1, *Appl. Environ. Microbiol. 67*, 713−720.
21. Otwinoski, Z., and Minor, W. (1997) Processing of X-ray diffraction data collected in oscillation mode, *Methods Enzymol. 276*, 307−326.
22. Brünger, A. T., Adams, P. D., Clore, G. M., Delano, W. L., Gros, P., Grosse-Kunstleve, R. W., Jiang, J.-S., Kuszewski, J., Nilges, N., Pannu, N. S., Read, R. J., Rice, L. M., Simonson, T., and Warren, G. L. (1998) Crystallography and NMR system (CNS): A new software system for macromolecular structure determination, *Acta Crystallogr. D54*, 905−921.
23. Laskowski, R. A., MacArthur, M. W., Moss, D. S., and Thornton, J. M. (1993) PROCHECK: A program to check the stereochemical quality of protein structures, *J. Appl. Crystallogr. 26*, 283−291.
24. Kabsch, W. (1976) A solution for the best rotation to relate two sets of vectors, *Acta Crystallogr. A32*, 922−923.
25. Collaborative Computational Project, Number 4 (1994) The CCP4 suite: Programs for protein crystallography, *Acta Crystallogr. D50*, 760−763.
26. Potterton, E., Briggs, P., Turkenburg, M., and Dodson, E. (2003) A graphical user interface to the CCP4 program suite, *Acta Crystallogr. D59*, 1131−1137.
27. Kraulis, P. J. (1991) MOLSCRIPT: A program to produce both detailed and schematic plots of protein structure, *J. Appl. Crystallogr. 24*, 946−950.
28. Merrit, E. A., and Murphy, M. E. P. (1994) RASTER3D Version 2.0. A program for photorealistic molecular graphics, *Acta Crystallogr. D50*, 869−873.
29. Esnouf, R. M. (1997) An extensively modified version of MolScript that includes greatly enhanced coloring capabilities, *J. Mol. Graphics Modell. 15*, 132−134.
30. Sanger, F., Nicklen, S., and Coulson, A. R. (1977) DNA sequencing with chain-terminating inhibitors, *Proc. Natl. Acad. Sci. U.S.A. 74*, 5463−5467.
31. Ausbel, F. M., Brent, R., Kingston, R. E., Moore, D. D., Seidman, J. G., Smith, J. A., and Struhl, K. (1987) *Current Protocols in Molecular Biology*, Wiley, New York.
32. Li, S., Kelly, S. J., Lamani, E., Ferraroni, M., and Jedrzejas, M. J. (2000) Structural basis of hyaluronan degradation by *Streptococcus pneumoniae* hyaluronate lyase, *EMBO J. 15*, 1228−1240.
33. Li, S., and Jedrzejas, M. J. (2001) Hyaluronan binding and degradation by *Streptococcus agalactiae* hyaluronate lyase, *J. Biol. Chem. 276*, 41407−41416.
34. Fethiere, J., Eggimann, B., and Cygler, M. (1999) Crystal structure of chondroitin AC lyase, a representative of a family of glycosaminoglycan degrading enzymes, *J. Mol. Biol. 288*, 635−647.
35. Huang, W., Lunin, V. V., Li, Y., Suzuki, S., Sugiura, N., Miyazono, H., and Cygler, M. (2003) Crystal structure of *Proteus vulgaris* chondroitin sulfate ABC lyase I at 1.9 Å resolution, *J. Mol. Biol. 328*, 623−634.
36. Akhtar, M. S., and Bhakuni, V. (2003) *Streptococcus pnermoniae* hyaluronate lyase contains two non-cooperative independent folding/unfolding structural domains: Characterization of functional domain and inhibitors of enzyme, *J. Biol. Chem. 278*, 25509−25516.
37. Kelly, S. J., Taylor, K. B., Li, S., and Jedrzejas, M. J. (2001) Kinetic properties of *Streptococcus pneumoniae* hyaluronate lyase, *Glycobiology 11*, 297−304.
38. Yoon, H.-J., Mikami, B., Hashimoto, W., and Murata, K. (1999) Crystal structure of alginate lyase A1-III from *Sphingomonas* species A1 at 1.78 Å resolution, *J. Mol. Biol. 290*, 505−514.
39. Aleshin, A. E., Feng, P.-H., Honzatko, R. B., and Reilly, P. J. (2003) Crystal structure and evolution of a prokaryotic glucoamylase, *J. Mol. Biol. 327*, 61−73.
40. Cronin, C. N., and Kirsch, J. F. (1988) Role of arginine-292 in the substrate specificity of aspartate aminotransferase as examined by site-directed mutagenesis, *Biochemistry 27*, 4572−4579.
41. Almo, S. C., Smith, D. L., Danishefsky, A. T., and Ringe, D. (1994) The structural basis for the altered substrate specificity of the R292D active site mutant of aspartate aminotransferase from *E. coli*, *Protein Eng. 7*, 405−412.

42. Okamoto, A., Higuchi, T., Hirotsu, K., Kuramitsu, S., and Kagamiyama. H. (1994) X-ray crystallographic study of pyridoxal 5′-phosphate-type aspartate aminotransferases from *Escherichia coli* in open and closed form, *J. Biochem. 116*, 95−107.
43. Levy, S., Schuyler, S. C., Maglothin, R. K., and Staehelin, L. A. (1996) Dynamic simulations of the molecular conformations of wild type and mutant xanthan polymers suggest that conformational differences may contribute to observed differences in viscosity, *Biopolymers 38*, 251−272.
44. Ruijssenaars, H. J., de Bont, J. A. M., and Hartmans, S. (1999) A pyruvated mannose-specific xanthan degradation by *Paenibacillus alginolyticus* XL-1, *Appl. Environ. Microbiol. 65*, 2446−2452.
45. Ahlgren, J. A. (1991) Purification and characterization of a pyruvated-mannose-specific xanthan lyase from heat-stable, salt-tolerant bacteria, *Appl. Environ. Microbiol. 57*, 2523−2528.

BI0619775